Nano Research
DOI 10.1007/s12274-013-0309-7
Research Article
ISSN 1998-0124
CN 11-5974/O4

Highly defective graphene: A key prototype of two-dimensional Anderson insulators

Aurélien Lherbier[1](✉), Stephan Roche[2,3], Oscar A. Restrepo[4], Yann-Michel Niquet[5], Arnaud Delcorte[4], and Jean-Christophe Charlier[1]

[1] *Université catholique de Louvain (UCL), Institute of Condensed Matter and Nanoscience (IMCN), NAPS-ETSF, Chemin des étoiles 8, 1348 Louvain-la-Neuve, Belgium*
[2] *CIN2 (ICN-CSIC) and Universitat Autónoma de Barcelona, Catalan Institute of Nanotechnology, Campus UAB, 08193 Bellaterra (Barcelona), Spain*
[3] *ICREA, Institució Catalana de Recerca i Estudis Avançats, 08070 Barcelona, Spain*
[4] *Université catholique de Louvain (UCL), Institute of Condensed Matter and Nanoscience (IMCN), BSMA, Place Croix du Sud 1 (Boltzmann), 1348 Louvain-la-Neuve, Belgium*
[5] *L_Sim, SP2M, UMR-E CEA/UJF-Grenoble 1, INAC, 17 rue des Martyrs, 38054 Grenoble Cedex 9, France*

Received: 3 December 2012
Revised: 15 March 2013
Accepted: 16 March 2013

KEYWORDS
graphene,
electronic transport,
Anderson insulators,
localization

ABSTRACT

Electronic structure and transport properties of highly defective two-dimensional (2D) sp^2 graphene are investigated theoretically. Classical molecular dynamics are used to generate large graphene planes containing a considerable amount of defects. Then, a tight-binding Hamiltonian validated by ab initio calculations is constructed in order to compute quantum transport within a real-space order-N Kubo–Greenwood approach. In contrast to pristine graphene, the highly defective sp^2 carbon sheets exhibit a high density of states at the charge neutrality point raising challenging questions concerning the electronic transport of associated charge carriers. The analysis of the electronic wavepacket dynamics actually reveals extremely strong multiple scattering effects giving rise to mean free paths as low as 1 nm and localization phenomena. Consequently, highly defective graphene is envisioned as a remarkable prototype of 2D Anderson insulating materials.

1 Introduction

Graphene's outstanding electronic and mechanical properties [1–3] are currently used to engineer novel types of flexible and transparent electrodes [4, 5]. However, the available large-scale graphene samples grown by chemical vapor deposition (CVD) remain rich in defects and grain boundaries which can limit the performances of related devices [6]. The detrimental effects of such structural imperfections on charge mobility are difficult to circumvent and require close inspection. Theoretically, the impact of extended lines of defects and of single structural defects (as produced by rapid thin-film growth or using ion-irradiation) has

Address correspondence to aurelien.lherbier@uclouvain.be

been now widely studied [7–12], revealing interesting features such as electron–hole transport asymmetry [13] due to the presence of defect-induced resonances.

Recently, using controlled electron irradiation, Kotakoski et al. [14] have reported on the possible engineering of a new two-dimensional (2D) amorphous carbon lattice. The latter is composed of sp^2-hybridized carbon atoms, arranged as a random tiling of the plane with polygons including four-membered rings. So far, only few studies, mostly theoretical [15–18], have examined this new allotrope of the sp^2 carbon family. A large increase of the density of states (DOS) at the charge neutrality point is an unvarying prediction concerning these amorphous carbon lattices. However, their transport properties are still debated. Based on a stochastic quenching method, these 2D amorphous carbon lattices have been suggested to show metallic behavior, suitable for transparent electrodes applications [17], while other approaches have reported on the presence of localized states [15] which should greatly inhibit the transport properties leading eventually to an insulating behavior. Therefore, this new carbon allotrope system deserves more detailed analysis to unravel accurately its electronic and transport properties.

In this article, a realistic model of this 2D amorphous carbon system is investigated, namely a highly defective graphene structure. In contrast to fully amorphous graphene membranes, highly defective graphene systems are composed of patches of highly defective regions together with reconstructed pristine areas. Here, such highly defective graphene structures are created using classical molecular dynamics simulations. Although the obtained defective graphene models also exhibit a high DOS close to the charge neutrality point (the Dirac point for pristine graphene), the resulting transport properties display features typical of a strong Anderson insulator, with elastic mean free paths below 1 nanometer, low mobilities on the order of 10–100 $cm^2 \cdot V^{-1} \cdot s^{-1}$ and considerable effects of quantum interference. Despite our calculations predicting that 2D highly defective carbon lattices are not the best suited graphene-based system for applications as conductive materials in electronic devices, the present study suggests that such highly defective graphene-based prototypes should offer intriguing possibilities to explore theoretically and experimentally the physics of 2D Anderson insulators.

2 Results and discussion

2.1 Highly defective graphene structure from classical molecular dynamics

The highly defective graphene (HDG) structures are generated by classical molecular dynamics (CMD) simulations. Starting from a pristine graphene square sheet (200 nm × 200 nm, i.e., ~1:5 × 10^6 carbon atoms), a small random in-plane displacement $\delta \boldsymbol{R}$ is applied to each atomic position with $|\delta \boldsymbol{R}| \leqslant d_{CC}/3$, $d_{CC} = 1.42$ Å being the carbon–carbon interatomic distance. This *randomized graphene sheet* serves as an input for the CMD calculation (Fig. 1(a)). The evolution of atomic positions are driven by an interatomic Tersoff-type potential (REBO) developed by Brenner et al. [19, 20]. In the CMD simulations, periodic boundary conditions are applied and, to promote the healing of highly unstable defects, a large window of thermostatic Langevin temperatures (T_L) from 0 K to 2,600 K is probed. The total number of carbon atoms being kept constant, the CMD simulations are hence performed in the context of the *canonical ensemble*. Moreover, in a first step, velocities along the perpendicular direction to the sheet are set to zero, thus confining the atoms in the plane. After 500 fs, the atomic positions do not change significantly anymore. The dynamics is however continued till 2,000 fs to allow the occurrence of low probability events. Then, a snapshot of the system is taken. A structural disorder model is obtained typically containing domains of strongly defective graphene together with preserved regions maintaining the local honeycomb lattice although slightly deformed (Fig. 1(b)). In a second step, another CMD simulation, with T_L fixed to 10 K, is conducted allowing out-of-plane deformations (Fig. 1(c)). A similar procedure has been applied in reference [17]. This last step can eventually yields to the ejection out-of-plane of a few atoms.

A huge variety of structural defects including some exotic ones can be observed in the defective graphene plane (as partially illustrated in Fig. 1(d)). These structural modifications consist of non-hexagonal

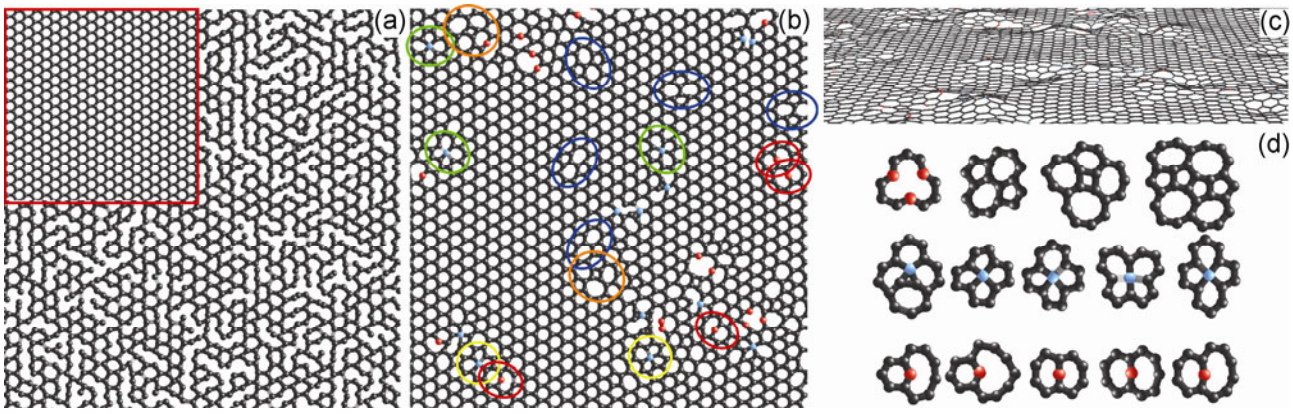

Figure 1 Geometry of highly defective graphene. (a) Randomized graphene layer (inset: starting pristine graphene layer) used as input for the CMD simulation. (b) Structure model of highly defective graphene following CMD at T_L = 1,200 K. Specific defects of the same type are indicated with circles of the same color. (c) Structure model after the second CMD simulation allowing out-of-plane deformations. The square piece of graphene presented in (a), (b) and (c) is only a small part of the whole system which is 200 nm × 200 nm. (d) Non-exhaustive list of the most frequently observed structural defects isolated from the plane. 2-, 3-, and 4-coordinated carbon atoms are depicted using red, black, and blue spheres, respectively.

rings, incorporating 2-, 3-, and/or 4-coordinated carbon atoms. Occasionally, dangling carbon atoms (1-coordinated) are generated but in extremely small quantity (discarded in subsequent transport calculations since they are particularly unstable), while 5-coordinated carbon atoms have never been observed. The 2-coordinated carbon atoms are observed in conjunction with dangling bonds or short linear atomic chains. Finally, 4-coordinated carbon atoms are mostly detected at the intersection of various membered rings. However, the number of low- and high-coordinated carbon atoms is found to decrease with Langevin temperature as depicted in Fig. 2(a). For instance, at T_L = 2,600 K, 2- and 4-coordinated carbon atoms represent less than 2% of the whole sheet. After the second CMD simulation, a tiny amount of carbon atoms (<0.0033%) are ejected from the plane, thus creating small holes in the sheet around which short atomic chains are occasionally observed. Consequently, after this second CMD simulation, slightly more 1-coordinated carbon atoms are counted as shown in Fig. 2(a) (dashed lines), although the general coordination number statistics are almost unchanged compared to the 2D approximation. Amongst the large variety of defects, some well-known defects are more frequently observed (such as Stone–Wales defects, vacancies), but also various forms of *double ring* defects composed of 6 or higher membered carbon rings (such as the 6–9, 6–10, 7–7, 7–8, and 7–9 defects displayed in the last row in Fig. 1(d)). Different topologies of planar 4-coordinated carbon with a 90° angle configuration (5555, 555-6, 55-66) are also detected for not too high T_L. Interestingly, these metastable geometries were predicted by Hoffmann et al. in 1970 [21] and have also been proposed to play a key role in the migration of vacancies in irradiated carbon nanotubes [22] and graphene [23]. The planar HDG structures obtained using the Brenner potential within CMD simulations can eventually lead to small internal stress inducing metastable carbon geometries such as the 4-coordinated carbon atoms. However, these metastable geometries tend to disappear by self-healing with increasing T_L. In addition, their small amount should not alter the following electronic transport results. The presence of a large number of pentagons and heptagons is expected to induce some puckering of the HDG layer [16]. However, using an accurate first principles-based stochastic quenching method, a recent study has predicted that the buckling amplitude should be small in amorphous graphene planes (1.7 A) due to "*an averaging of defect-induced buckling forces*" [17]. Indeed, out-of-plane deformations induced locally by pentagons and heptagons tend to annihilate themselves, as occurs for instance in a 555-777 divacancy defect whose stable geometry is planar [8, 4]. The much larger system obtained here is slightly different

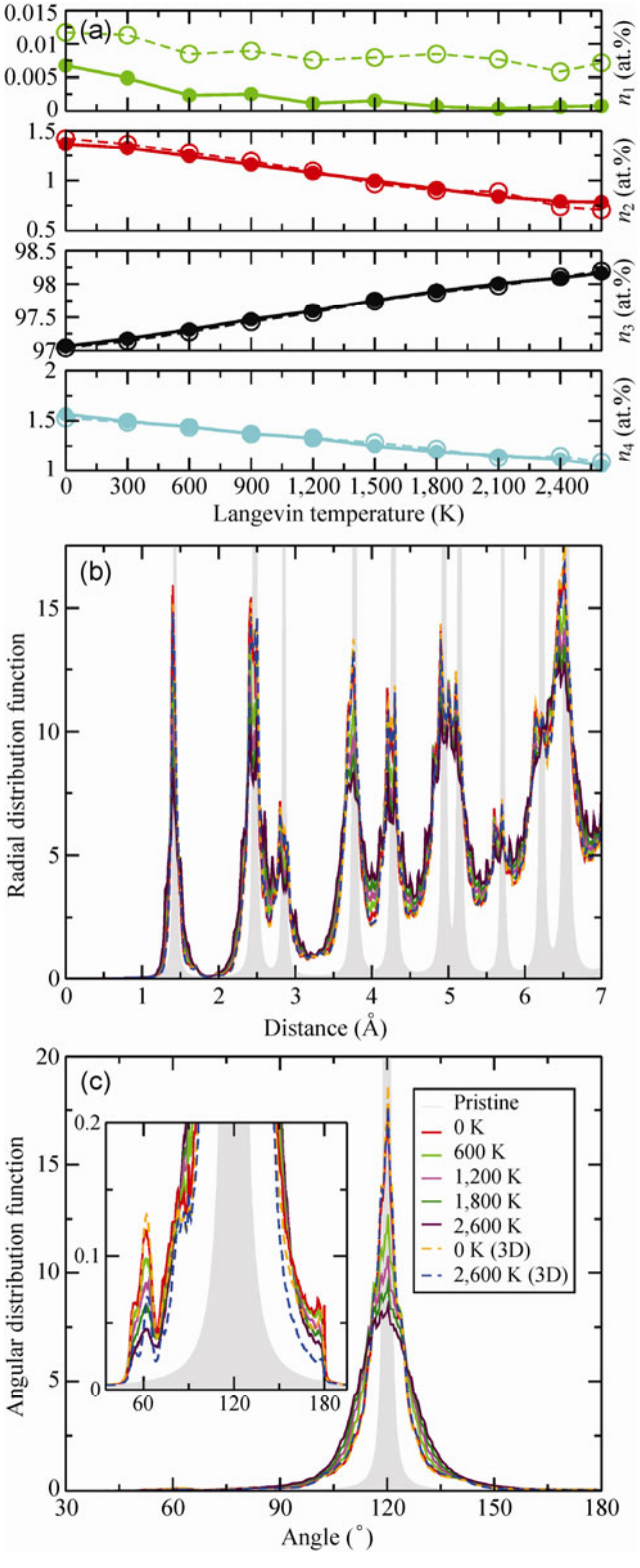

Figure 2 (a) Percentage of carbon atoms exhibiting coordination numbers from 1 (n_1) to 4 (n_4) as a function of T_L. Radial (b) and angular (c) distribution functions of pristine graphene (gray filled curves) and HDG as a function of T_L. Results after the 3D CMD are plotted in dashed lines.

from those in Refs. [15–17], since it is not completely amorphous and contains randomly distributed ordered areas[1]. In the present case, the maximum deviation from the plane is estimated to be ~2.5 A. The buckling is mostly observed in regions containing non 3-coordinated carbon atoms, while an essentially reconstructed honeycomb lattice area appears (Fig. 2(c)). Nevertheless, any corrugation of the HDG would eventually be reduced by a flat underlying substrate such as hexagonal boron nitride [24, 25].

The HDG sheets can be further characterized by analyzing the radial and angular distribution functions (RDF/ADF). In principle, the RDF of pristine graphene presents Dirac peaks at the 1st, 2nd, 3rd … nearest neighbors (-nn) distances. However, these peaks have been broadened by a Lorentzian function in Fig. 2(b) to enhance the readability of the plots. The same broadening has been used for the RDF of the HDG. However, an additional broadening can be observed, which is rather small for the 1st-nn peak, but increases with distance (i.e., for next-nn). This is a clear signature of a relative amorphization of the system. The broadening is also found to increase with T_L [2] in 2D CMD simulations, while for subsequent 3D CMD simulations (dashed lines in Figs. 2(b) and 2(c)), the RDF curves are all similar to the 2D CMD results obtained for $T_L = 0$ K. The ADF of the pristine graphene depicted in Fig. 2(c), is composed of a single peak at 120°, while in the HDG layer, other small peaks emerge at 60° and 180° due to the incorporation of defects (see inset). A tiny peak at 90°, resulting from the few 4-coordinated carbon atoms, is also observed at low T_L but disappears for higher T_L. In addition, the main peak around 120° is clearly broadened. Again, this broadening is larger for higher T_L, which demonstrates the more pronounced disordered character for higher T_L. However, as observed for the RDF, when performing the final 3D CMD the ADF curves go back to the result of 2D CMD at $T_L = 0$ K. In the following, the electronic and transport properties of HDG planes will be investigated using a *tight-binding* (TB) framework

[1] To avoid misleading comparisons between highly defective graphene and amorphous graphene, the first terminology has been preferred and used along the manuscript.

[2] For a fixed TL, RDF/ADF and transport calculations are performed using only one HDG layer. However, an intrinsic average of the disorder exists due to the large system size.

together with an efficient real-space Kubo–Greenwood formalism. The presence of a large variety of defects together with buckling renders the TB parameterization very tedious. Therefore, since RDF and ADF of strictly 2D HDG and buckled HDG exhibit about the same coordination statistics, the electronic and transport properties will be computed in 2D HDG structures for the sake of simplicity.

2.2 Electronic properties

An empirical π–π^* orthogonal TB model [26] was used to explore the electronic properties of HDG. The essential ingredients of the model are a hopping term $\gamma(d) = \gamma_0 \exp(-3.37\ (d/d_{CC} - 1))$, with $\gamma_0 = -3.0933$ eV, for p_z orbitals separated by up to $d = 5$ Å one from each other, while the onsite energy is set to $\varepsilon_{pz} = 0.79745$ eV so that the Dirac point lies at 0 eV. A negative sign is added to $\gamma(d)$ for 2nd-nn, as an effect of orthogonality constraints. Figure 3 displays the DOS obtained for pristine graphene using the present TB model, which is in good agreement with a 3rd-nn π–π^* orthogonal TB model validated by *ab initio* calculations [13]. The DOS of HDG obtained at different T_L are also presented. A transition from a zero-gap semiconductor to a metallic-like phase is observed. Indeed, in HDG, a large increase of DOS is observed near the charge neutrality point. This increase of DOS can actually be explained by an overlap of numerous resonances induced by the presence of a huge number of

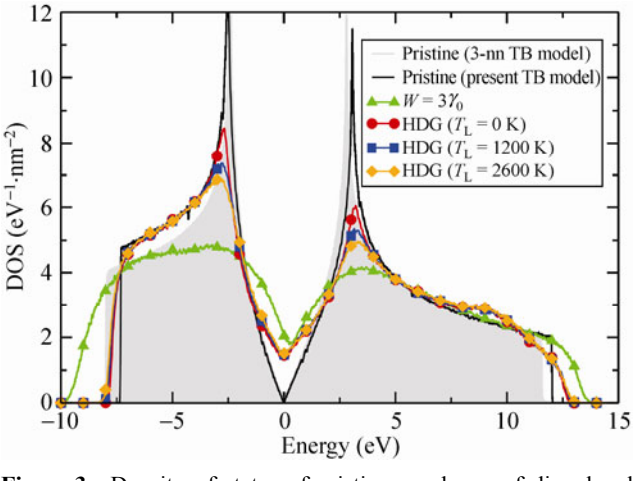

Figure 3 Density of states of pristine graphene, of disordered graphene ($W = 3\gamma_0$), and of three HDG layers obtained using different T_L.

structural defects of various natures [27]. Meanwhile, a smoothening of the two van Hove singularities is noticed on the DOS of HDG. These two features are typical of a strong Anderson disorder [28]. The latter is a well-known academic disorder model which consists of applying random fluctuations of the onsite energies: $\delta\varepsilon_{pz} = [-W/2, W/2]$. For comparison, the DOS of a graphene plane subjected to Anderson disorder using $W = 3\gamma_0$ (strong disorder) is also presented in Fig. 3 (green line with triangles). In that case, the van Hove singularities as well as the outer part of the spectrum are even more smoothed out because the Anderson disorder for $W = 3\gamma_0$ impacts the entire spectrum while for HDG planes, the various structural defects produce mainly energy resonances close to the Dirac point.

2.3 Electronic transport

The transport properties of the HDG layers are computed from the dynamics of electronic wavepackets with an order-N Kubo–Greenwood method [13, 28–33]. In this technique, the key quantity is time evolution of the diffusion coefficient ($D(E,t)$) from which the transport properties are explored. At very short times, the wavepacket dynamics is quasi-ballistic and $D(E,t)$ is linear in time. Then it becomes diffusive as the carriers get scattered by the disorder, and $D(E,t)$ reaches a maximum value from which we extract the mean free path ($l_e(E)$), the semiclassical conductivity ($\sigma_{sc}(E)$) and the mobility ($\mu(E)$) (see Methods section). At even longer times, localization due to multiple scattering events per carrier causes $D(E,t)$ to decrease.

In HDG, the computed mean free path is found to be weakly dependent on the energy (Fig. 4(a)), being almost constant ($l_e \sim 0.5$–1.5 nm ~ 4–$10\ d_{CC}$) over a large window ([–4,+4] eV). In Fig. 4(c), the charge carrier mobility derived from $\mu(E) = \sigma_{sc}(E)/(en(E))$ ($n(E)$ being the carrier density) is found to be of the order of 10–100 $cm^2 \cdot V^{-1} \cdot s^{-1}$ which is 2–3 orders of magnitude smaller than the experimental measurements on usual graphene samples [24, 34]. Figure 4(e) presents the semiclassical conductivity of the HDG sheet as a function of charge carrier energy. At the Dirac point, σ_{sc} exhibits a minimal value slightly above the universal minimum conductivity $\sigma_{sc}^{min} = 4e^2/\pi h$ predicted for a

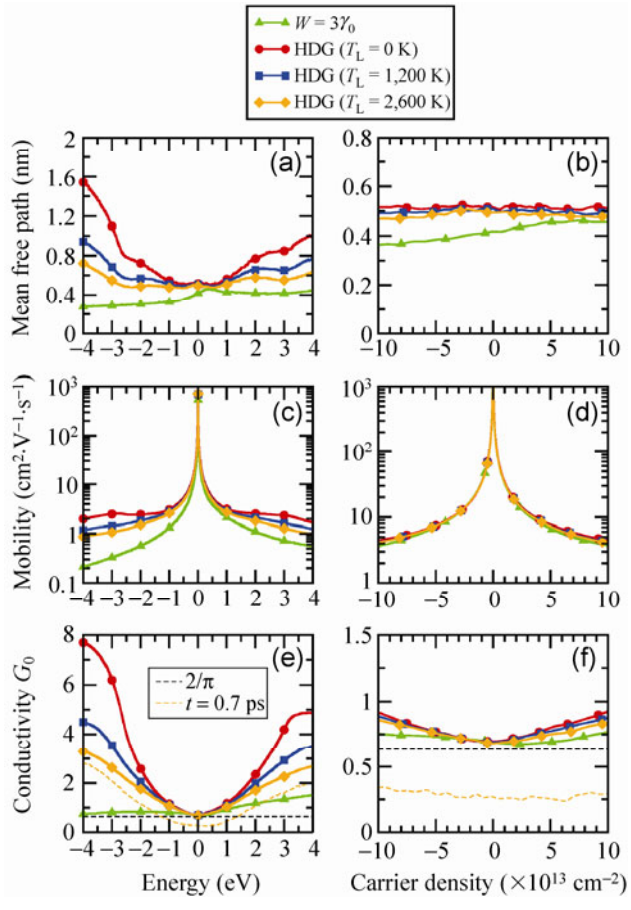

Figure 4 Transport properties of disordered graphene ($W = 3\gamma_0$) and of HDG obtained for three different T_L. (a) and (b) Electron/hole mean free paths. (c) and (d) Electron/hole mobilities. (e) and (f) Electron/hole conductivities. (a), (c), and (e) are given as a function of energy while (b), (d), (f) are given as a function of carrier density (negative densities corresponding to holes).

short range disorder potential, and whose origin is now well established [35–39]. Our results demonstrate that such a value could also be measured in a HDG at room temperature [1]. The mean free paths, the mobilities, and the conductivities in HDG are also plotted as a function of the charge carrier density in Figs. 4(b), 4(d) and 4(f) respectively. Close to the Dirac point, the values of $l_e(E)$, $\mu(E)$ and $\sigma_{sc}(E)$ obtained for a strong Anderson disorder ($W = 3\gamma_0$) are found very similar to the ones observed in the present HDG layers (see green lines with triangle symbols in Fig. 4).

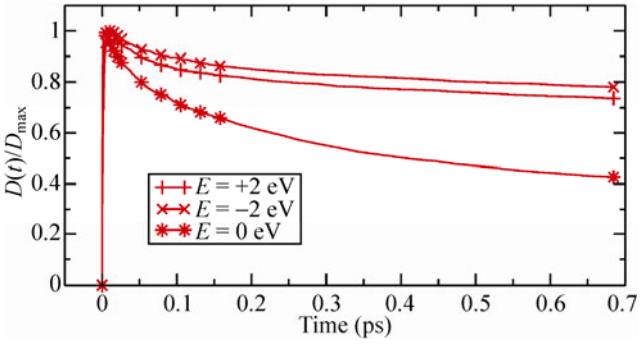

Figure 5 Normalized diffusion coefficient $D(t)/D_{max}$ in HDG obtained at $T_L = 0$ K and for three different energies $E = +2$, -2, and 0 eV (plus, crosses, and stars signs).

2.4 Localization effects

Due to the predicted short mean free paths, strong contributions of quantum interferences are expected at low temperatures. Compelling evidence of such interferences are exhibited by the time-dependence of the ratio $D(t)/D_{max}$. Figure 5 illustrates this ratio at three different energies (close to/far from the Dirac point). $D(t)/D_{max}$ quickly decays because of strong localization effects, suggesting a very short localization length ξ. Using the scaling theory of localization [40], ξ can be actually estimated from $\xi(E) = \sqrt{2}\, l_e(E) \cdot \exp(\pi h \sigma_{sc}(E)/2e^2)$. From our calculations, a value of $\xi \sim 5$ nm is estimated for $E = 0$ eV (where $\sigma_{sc} = \sigma_{sc}^{min}$), which appears to be extremely short. Moreover, for E in [–1,+1] eV, ξ is predicted to be smaller than 20 nm which is much shorter than for weakly disordered (e.g., doped) graphene [41]. The build-up of quantum interference beyond the short-time/short-length diffusive regime localizes the carriers and decreases the actual (quantum) conductivity of the system in large HDG samples (or equivalently at long times in our calculations). As an illustration, the quantum conductivity computed for a HDG layer ($T_L = 2600$ K) from the diffusivity at a longer time $t = 0.7$ ps [2] is plotted with a dashed-dotted line in Figs. 4(e) and 4(f). It is already significantly lower than σ_{sc} computed from D_{max} obtained at shorter times. At low temperatures, the electron–phonon scattering cannot efficiently break phase coherence, so the conductivity of HDG layers is expected to decrease exponentially with size (and

[1] The mobility and the conductivity have been computed using a Fermi–Dirac temperature of $T_F = 300$ K which essentially smoothes out the quantities obtained at 0 K.

[2] The time-dependent quantum conductivity $\sigma(E,t)$ is computed from $\sigma(E,t) = 1/4e^2\rho(E)D(E,t)$.

eventually vanish) beyond a few ξ, i.e., at most a few tens of nanometers. Localization should also lead to an easily observable variable range hopping behavior in the temperature dependence of the conductivity. Similar strong localization effects are obtained in the case of an Anderson disorder model. Eventually, the small puckering, as obtained in the 3D CMD simulations, would introduce slight additional sp^3 hybridization of carbon atoms, which is expected to increase the overall disorder strength and reinforce the present conclusion concerning the Anderson insulating behavior of HDG.

3 Conclusions

Large-sized highly defective graphene sheets generated by molecular dynamics exhibit enhanced densities of states close to the charge neutrality point, together with very short mean free paths (below 1 nm), low mobilities and strong localization effects. These highly defective graphene sheets are therefore suggested to become a genuine playground for fundamental exploration of Anderson localization phenomena in 2D systems. Raman analysis [42, 43] and low temperature transport measurements [44, 45] in such sp^2 *Anderson insulating* amorphous graphene layers would be desirable to confirm those predictions.

4 Methods

A real-space order-N Kubo–Greenwood approach is employed to compute the different transport properties. The latter are inferred from the dynamics of the wavepacket propagation. This dynamics is monitored through the time-dependent diffusion coefficient $D(E,t) = \Delta R^2(E,t)/t$, with E the energy of the carriers, $\Delta R^2 = \Delta X^2 + \Delta Y^2$, and $\Delta X^2(E,t) = \mathrm{Tr}[\delta(E–H)\,|X(t)–X(0)\,|^2]/\mathrm{Tr}[\delta(E–H)]$ the quadratic spreading along the x direction. Tr is the trace over p_z orbitals and $\mathrm{Tr}[\delta(E–H)]/S = \rho(E)$ is the total DOS (per unit of area S). The time-dependent Schrödinger equation is solved up to $t = 700$ fs thanks to an efficient expansion of the time evolution operator in a basis of Chebyshev polynomials ($U(t) = \prod_{n=0}^{N-1} \exp(iH\Delta t/\hbar)$ with Δt the time step). The time evolution operator $U(t)$ is used to compute both position operators $X(t)$ and $Y(t)$, expressed in the Heisenberg representation ($X(t) = U^{\dagger}(t)X(0)U(t)$). Transport calculations are averaged over many runs with different initial random phase wavepackets. At very short times, the wavepacket dynamics is quasi-ballistic, so that $D(E,t) \sim v^2(E)t$, where $v(E)$ is the carrier velocity. Then it becomes diffusive as the carriers get scattered by the disorder, and $D(E,t)$ reaches a maximum value $D_{max}(E) = 2v(E)l_e(E)$, where $l_e(E)$ is the mean free path. The semiclassical conductivity then reads $\sigma_{sc}(E) = \frac{1}{4}e^2\rho(E)D_{max}(E)$. At even longer times, localization due to multiple scattering events per carrier causes $D(E,t)$ to decrease.

In the present study, the Anderson disorder model (white noise potential) commonly used in the TB framework is likened to HDG layers. Random fluctuations ($\delta\varepsilon_{pz}$) are imposed on all onsite energies thus affecting the diagonal of the TB Hamiltonian. In such a model, the disorder strength is given by a single parameter W, which can be tuned from very small to high energies, or equivalently from weak to strong disorder. The onsite fluctuations terms are random but constrained within a range of $[–W/2,W/2]$. Usually, when the disorder strength W exceeds the width of the electronic spectrum of the material, the disorder is considered as very strong since it can alter the whole spectrum. In the present case, $W = 3\gamma_0 \sim 9$ eV is a quite strong disorder for graphene (π–π^* model). For more details, the reader is referred to a previous study [28].

Acknowledgements

J. -C. C., A. D., and A. L. acknowledge financial support from the Belgium FNRS. S. R. acknowledges the Spanish Ministry for financial support through the project MAT2012-33911. This work is connected to the ARC Graphene Nano-electromechanics (N.° 11/16-037), the ETSF e-I3 project (N.° 211956), and the NANOSIM-GRAPHENE (ANR-09-NANO-016-01). Computational resources are provided by the UCL-CISM. Free access to the SPUT code was granted by Prof. B. J. Garrison.

References

[1] Kim, K. S.; Zhao, Y.; Jang, H.; Lee, S. Y.; Kim, J. M.; Kim, K. S.; Ahn, J.-H.; Kim, P.; Choi, J.-Y.; Hong, B. H. Large-scale

pattern growth of graphene films for stretchable transparent electrodes. *Nature* **2009**, *457*, 706–710.

[2] Novoselov, K. S. Nobel lecture: Graphene: Materials in the flatland. *Rev. Mod. Phys.* **2011**, *83*, 837–849.

[3] de Heer, W. A.; Berger, C.; Wu, X.; First, P. N.; Conrad, E. H.; Li, X.; Li, T.; Sprinkle, M.; Hass, J.; Sadowski, M. L.; Potemski, M.; Martinez, G. Epitaxial graphene. *Solid State Commun*. **2007**, *143*, 92–100.

[4] Wang, X.; Zhi, L.; Müllen, K. Transparent, conductive graphene electrodes for dye-sensitized solar cells. *Nano Lett.* **2008**, *8*, 323–327.

[5] Bae, S.; Kim, H.; Lee, Y.; Xu, X.; Park, J.-S.; Zheng, Y.; Balakrishnan, J.; Lei, T.; Kim, H. R.; Song, Y. I.; et al. Roll-to-roll production of 30-inch graphene films for transparent electrodes. *Nat. Nanotechnol.* **2010**, *5*, 574–578.

[6] Ferreira, A.; Xu, X.; Tan, C. -L.; Bae, S. -K.; Peres, N. M. R.; Hong, B. -H.; Özyilmaz, B.; Castro Neto, A. H. Transport properties of graphene with one-dimensional charge defects. *Eur. Phys. Lett.* **2011**, *94*, 28003–28008.

[7] Krasheninnikov, A. V.; Banhart, F. Engineering of nano-structured carbon materials with electron or ion beams. *Nat. Mater.* **2007**, *6*, 723–733.

[8] Banhart, F.; Kotakoski, J.; Krasheninnikov, A. V. Structural defects in graphene. *ACS Nano* **2011**, *5*, 26–41.

[9] Cockayne, E.; Rutter, G. M.; Guisinger, N. P.; Crain, J. N.; First, P. N.; Stroscio, J. A. Grain boundary loops in graphene. *Phys. Rev. B* **2011**, *83*, 195425.

[10] Botello-Méndez, A. R.; Declerck, X.; Terrones, M.; Terrones, H.; Charlier, J.-C. One-dimensional extended lines of divacancy defects in graphene. *Nanoscale* **2011**, *3*, 2868–2872.

[11] Lusk, M. T.; Wu, D. T.; Carr, L. D. Graphene nano-engineering and the inverse Stone–Thrower–Wales defect. *Phys. Rev. B* **2010**, *81*, 155444.

[12] Yazyev, O. V.; Louie, S. G. Electronic transport in polycrystalline graphene. *Nat. Mater.* **2010**, *9*, 806–809.

[13] Lherbier, A.; Dubois, S. M.-M.; Declerck, X.; Roche, S.; Niquet, Y. M.; Charlier, J.-C. Two-dimensional graphene with structural defects: Elastic mean free path, minimum conductivity, and Anderson transition. *Phys. Rev. Lett.* **2011**, *106*, 046803.

[14] Kotakoski, J.; Krasheninnikov, A. V.; Kaiser, U.; Meyer, J. C. From point defects in graphene to two-dimensional amorphous carbon. *Phys. Rev. Lett.* **2011**, *106*, 105505.

[15] Kapko, V.; Drabold, D. A.; Thorpe, M. F. Electronic structure of a realistic model of amorphous graphene. *Phys. Stat. Solidi B* **2010**, *247*, 1197–1200.

[16] Li, Y.; Inam, F.; Kumar, A.; Thorpe, M. F.; Drabold, D. A. Pentagonal puckering in a sheet of amorphous graphene. *Phys. Stat. Solidi B* **2011**, *248*, 2082–2086.

[17] Holmström, E.; Fransson, J.; Eriksson, O.; Lizárraga, R.; Sanyal, B.; Bhandary, S.; Katsnelson, M. I. Disorder-induced metallicity in amorphous graphene. *Phys. Rev. B* **2011**, *84*, 205414.

[18] Tuan, D. V.; Kumar, A.; Roche, S.; Ortmann, F.; Thorpe, M. F.; Ordejon, P. Insulating behavior of an amorphous graphene membrane. *Phys. Rev. B* **2012**, *86*, 121408.

[19] Brenner, D. W.; Shenderova, O. A.; Harrison, J. A.; Stuart, S. J.; Ni, B.; Sinnott, S. B. A second-generation reactive empirical bond order (REBO) potential energy expression for hydrocarbons. *J. Phys. Cond. Matt.* **2002**, *14*, 783–802.

[20] Stuart, S. J.; Tutein, A. B.; Harrison, J. A. A reactive potential for hydrocarbons with intermolecular interactions. *J. Chem. Phys.* **2000**, *112*, 6472–6486.

[21] Hoffmann, R.; Alder, R. W.; Wilcox, C. F. Planar tetracoordinate carbon. *J. Am. Chem. Soc.* **1970**, *92*, 4992–4993.

[22] Ajayan, P. M.; Ravikumar, V.; Charlier, J.-C. Surface reconstructions and dimensional changes in single-walled carbon nanotubes. *Phys. Rev. Lett.* **1998**, *81*, 1437–1440.

[23] Wang, B.; Puzyrev, Y.; Pantelides, S. T. Strain enhanced defect reactivity at grain boundaries in polycrystalline graphene. *Carbon* **2011**, *49*, 3983–3988.

[24] Dean, C. R.; Young, A. F.; Meric, I.; Lee, C.; Wang, L.; Sorgenfrei, S.; Watanabe, K.; Taniguchi, T.; Kim. P.; Shepard, K. L.; et al. Boron nitride substrates for high-quality graphene electronics. *Nat. Nanotechnol.* **2010**, *5*, 722–726.

[25] Xue, J.; Sanchez-Yamagishi, J.; Bulmash, D.; Jacquod, P.; Deshpande, A.; Watanabe, K.; Taniguchi, T.; Jarillo-Herrero, P.; LeRoy, B. J. Scanning tunnelling microscopy and spectroscopy of ultra-flat graphene on hexagonal boron nitride. *Nat. Mater.* **2011**, *10*, 282–285.

[26] Pereira, V. M.; Castro Neto, A. H.; Peres, N. M. R. Tight-binding approach to uniaxial strain in graphene. *Phys. Rev. B* **2009**, *80*, 045401.

[27] Lherbier, A.; Dubois, S. M.-M.; Declerck, X.; Niquet, Y. M.; Roche, S.; Charlier, J.-C. Transport properties of graphene containing structural defects. *Phys. Rev. B* **2012**, *86*, 075402.

[28] Lherbier, A.; Biel, B.; Niquet, Y. M.; Roche, S. Transport length scales in disordered graphene-based materials: Strong localization regimes and dimensionality effects. *Phys. Rev. Lett.* **2008**, *100*, 036803.

[29] Roche, S.; Mayou, D. Conductivity of quasiperiodic systems: A numerical study. *Phys. Rev. Lett.* **1997**, *79*, 2518–2521.

[30] Roche, S. Quantum transport by means of O(N) real-space methods. *Phys. Rev. B* **1999**, *59*, 2284–2291.

[31] Ishii, H.; Triozon, F.; Kobayashi, N.; Hirose, K.; Roche, S. Charge transport in carbon nanotubes based materials: A Kubo–Greenwood computational approach. *C. R. Phys.* **2009**, *10*, 283–296.

[32] Leconte, N.; Moser, J.; Ordejón, P.; Tao, H.; Lherbier, A.; Bachtold, A.; Alsina, F.; Sotomayor Torres, C. M.; Charlier, J.-C.; Roche, S. Damaging graphene with ozone treatment: A chemically tunable metal-insulator transition. *ACS Nano* **2010**, *4*, 4033–4038.

[33] Radchenko, T. M.; Shylau, A. A.; Zozoulenko, I. V. Influence of correlated impurities on conductivity of graphene sheets: Time-dependent real-space Kubo approach. *Phys. Rev. B* **2012**, *86*, 035418.

[34] Tan, Y.-W.; Zhang, Y.; Bolotin, K.; Zhao, Y.; Adam, S.; Hwang, E. H.; Das Sarma, S.; Stormer, H. L.; Kim, P. Measurement of scattering rate and minimum conductivity in graphene. *Phys. Rev. Lett.* **2007**, *99*, 246803.

[35] Shon, N. H.; Ando, T. Quantum transport in two-dimensional graphite system. *J. Phys. Soc. Jpn.* **1998**, *67*, 2421–2429.

[36] Peres, N. M. R.; Guinea, F.; Castro Neto, A. H. Electronic properties of disordered two-dimensional carbon. *Phys. Rev. B* **2006**, *73*, 125411.

[37] Ostrovsky, P. M.; Gornyi, I. V.; Mirlin, A. D. Electron transport in disordered graphene. *Phys. Rev. B* **2006**, *74*, 235443.

[38] Nomura, K.; MacDonald, A. H. Quantum transport of massless Dirac fermions. *Phys. Rev. Lett.* **2007**, *98*, 076602.

[39] Geim, A. K.; Novoselov, K. S. The rise of graphene. *Nat. Mater.* **2007**, *6*, 183–191.

[40] Lee, P. A.; Ramakrishnan, T. V. Disordered electronic systems. *Rev. Mod. Phys.* **1985**, *57*, 287–337.

[41] Lherbier, A.; Blase, X.; Niquet, Y. M.; Triozon, F.; Roche, S. Charge transport in chemically doped 2D graphene. *Phys. Rev. Lett.* **2008**, *101*, 036808.

[42] Ferrari, A. C.; Meyer, J. C.; Scardaci, V.; Casiraghi, C.; Lazzeri, M.; Mauri, F.; Piscanec, S.; Jiang, D.; Novoselov, K. S.; Roth, S.; et al. Raman spectrum of graphene and graphene layers. *Phys. Rev. Lett.* **2006**, *97*, 87401.

[43] Casiraghi, C.; Hartschuh, A.; Qian, H.; Piscanec, S.; Georgi, C.; Fasoli, A.; Novoselov, K. S.; Basko, D. M.; Ferrari, A. C. Raman spectroscopy of graphene edges. *Nano Lett.* **2009**, *9*, 1433–1441.

[44] Liu, G.; Teweldebrhan, D.; Balandin, A. A.; Tuning of graphene properties via controlled exposure to electron beams. *IEEE Trans. Nanotechnol.* **2011**, *10*, 865–870.

[45] Teweldebrhan, D.; Balandin, A. A. Modification of graphene properties due to electron beam irradiation. *Appl. Phys. Lett.* **2009**, *94*, 013101.

Table of contents

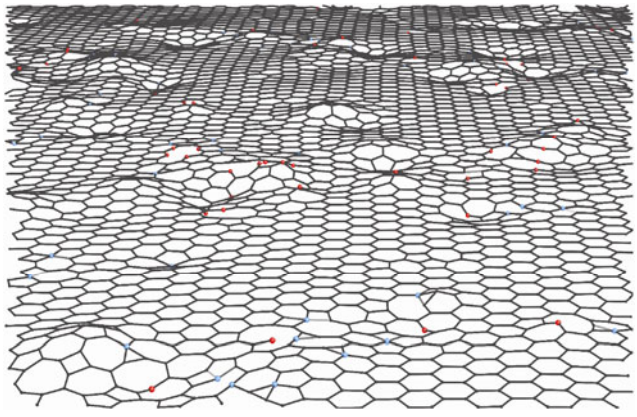

We provide theoretical predictions of the electronic structure and transport properties in highly defective graphene (HDG). Simulations reveal mean free paths as low as 1 nm and strong Anderson localization phenomena, suggesting HDG as a remarkable prototype of a two-dimensional Anderson insulator.